Bioactive Materials 3 (2018) 426–433

Contents lists available at ScienceDirect

Bioactive Materials

journal homepage: http://www.keaipublishing.com/biomat

The effect of applied voltages on the structure, apatite-inducing ability and antibacterial ability of micro arc oxidation coating formed on titanium surface

Qing Du[a,b], Daqing Wei[a,b,c,**], Yaming Wang[a,b,*,1], Su Cheng[d], Shang Liu[a,b], Yu Zhou[a,b], Dechang Jia[a,b]

[a] Institute for Advanced Ceramics, Department of Materials Science and Engineering, Harbin Institute of Technology, Harbin, 150001, China
[b] Key Laboratory of Advanced Structural-Functional Integration Materials & Green Manufacturing Technology, Harbin Institute of Technology, Harbin, 150001, China
[c] Center of Analysis and Measurement, Harbin Institute of Technology, Harbin, 150001, China
[d] Department of Mechanical Engineering, School of Architecture and Civil Engineering, Harbin University of Science and Technology, Harbin, 150001, China

ARTICLE INFO

Keywords:
Micro arc oxidation
Zn element
Applied voltage
Apatite-inducing ability
Antibacterial ability

ABSTRACT

The micro arc oxidation (MAO) coatings with different concentrations of Ca, P and Zn elements are successfully formed on the titanium substrate at the different applied voltages. After MAO treatment, the MAO coating exhibits the porous surface structure and composed of anatase and rutile TiO_2 phases. Meanwhile, the average size and density of micro-pores on the MAO coatings have been modified via the adjusting the applied voltages. In addition, the contents of the incorporated elements such as Zn, Ca and P elements in the MAO coatings have been optimized. The bonding strength test results reveal that the MAO coating shows higher bonding strength, which is up to 45 ± 5 MPa. Compared to the pure Ti plate, the MAO coating formed at 350 and 400 V show good apatite-inducing ability. Meanwhile, the MAO coating containing Zn, Ca and P elements have better antibacterial ability for *E.coli* and *S.aureus*. Thus, the incorporation of Zn, Ca and P elements was an effective method to improve the antibacterial ability. Moreover, the concentrations of Zn, Ca and P elements could be adjusted with the changing of the applied voltages. As a result, the enhancement of the antibacterial ability on the MAO coating surfaces was depended on the comprehensive effect of the incorporated elements and the surface property of MAO coatings.

1. Introduction

Titanium and its alloys are widely applied to the repair and replacement of hard tissue [1,2] (bone and teeth) due to the good corrosion resistance and excellent biocompatibility [3]. However, the bacteria infection could occur after the surgery, which could affect the repairment of bone defect and the success of implant surgery [4].

In order to improve the antibacterial ability of titanium and its alloys, some modified methods including sol-gel method [5,6], electrochemical deposition method [7–10] and micro arc oxidation method [10–16] are used to fabricate the coating containing antibacterial elements such as Ag, Zn and Cu elements.

According to previous studies [4–8,17–21], it was well known that the Ag and Cu elements possess good antibacterial ability. However, their potential cytotoxicity must be considered. Among the antibacterial elements, the Zinc element has poor cytotoxicity [14] and could improve the antibacterial activity of titanium implants [22,23]. Meanwhile, the previous studies [11,13,14] have reported that the Zn element has relatively weak antibacterial ability, which can be enhanced via increasing the amounts of Zn elements. The concentrations of Zn elements in the coatings are adjusted via increasing the concentrations of electrolyte during the sol-gel and electrochemical disposition process [24]. However, the bonding strength between the antibacterial coating and titanium substrate is poor, which restricts its application.

Owing to the high bonding strength and composition-controlled property, the micro arc oxidation (MAO) is an effective method to adjust the concentrations of Zn element [10,11,13]. Moreover, the

Peer review under responsibility of KeAi Communications Co., Ltd.
* Corresponding author. Institute for Advanced Ceramics, Science Park, Harbin Institute of Technology, Yikuang Street, Harbin, 150080, China.
** Corresponding author. Institute for Advanced Ceramics, Science Park, Harbin Institute of Technology, Yikuang Street, Harbin, 150080, China.
E-mail addresses: daqingwei@hit.edu.cn (D. Wei), wangyaming@hit.edu.cn (Y. Wang).
[1] Postal address: P.O.Box 3022#, Institute for Advanced Ceramics, Science Park, Harbin Institute of Technology, NO.2 Yi kuang Street, Harbin, 150080, PR China.

https://doi.org/10.1016/j.bioactmat.2018.06.001
Received 4 January 2018; Received in revised form 22 June 2018; Accepted 22 June 2018
Available online 02 July 2018

properties and composition concentrations of the MAO coatings are mainly affected by some parameters including the applied voltage, duty cycle, pulse frequency and oxidize time. In this work, the Zn-incorporated MAO coatings are fabricated on the titanium at the different applied voltage, and the contents of Zn element in the MAO coatings are adjusted by changing the applied voltages. The surface and cross-section structure, apatite-inducing ability and antibacterial ability of the Zn-incorporated MAO coating formed at the different applied voltage are studied.

2. Experimental procedure

2.1. Micro arc oxidation (MAO) treatment

In the MAO process, the pure Ti plates ($10 \times 10 \times 1\ mm^3$) are used as the anodes, and the stainless steel plates are used as cathodes in an electrolytic bath. The pure Ti plates are ground with abrasive papers of 200#, 400#, 600# and 800#, then ultrasonically washed with acetone and distilled water for three times, respectively, then dried at 40 °C. The electrolyte is prepared by the dissolving the EDTA-2Na (15 g), Ca$(CH_3COO)_2{\cdot}H_2O$ (8.8 g), Ca$(H_2PO_4){\cdot}H_2O$ (6.3 g), $Na_2SiO_3{\cdot}9H_2O$ (7.1 g), NaOH (5 g), H_2O_2 (6 mL) and Zn$(CH_3COO)_2$ (8.5 g) in 1 L deionized water. The applied voltage was set as 350, 400, 450 and 500 V for MAO experiment. The pulse frequency, duty cycle and oxidized time are set at 600 Hz, 8% and 7min, respectively. The labels of MAO coatings formed at the different voltages are shown in Table 1.

2.2. Simulated body fluid (SBF) immersion

To evaluate the apatite-inducing ability, the samples are immersed in the 30 mL simulated body fluid (SBF) [25] for 14 and 21days, and the SBF are refreshed every other day. The SBF is prepared by the dissolving of NaCl (8.036 g), $NaHCO_3$ (0.352 g), KCl (0.225 g), $K_2HPO_4{\cdot}3H_2O$ (0.23 g), $MgCl_2{\cdot}6H_2O$ (0.311 g), $CaCl_2$ (0.293 g), Na_2SO_4 (0.072 g) in 1 L deionized water. In the following, the SBF solutions are buffered at pH 7.4 with the Tris-hydroxymethylaminomethane ($(CH_2OH)_3CNH_2$) (6.063 g L^{-1}) and 1 mol/L HCl (40 mL) at 37 °C.

2.3. Structure characterization

2.3.1. X-ray diffraction (XRD)

The phase compositions of the samples were analyzed by X-ray diffraction (XRD, D/max-γB, Japan) using a CuKα radiation with a continuous scanning mode at a rate of 4°·min^{-1}. And the scanning range is from 10° to 90°. The accelerating voltage and current are set at 40 kV and 50 mV.

2.3.2. Scanning electron microscopy (SEM) and energy dispersive X-ray spectroscopy (EDS)

Scanning electron microscopy (SEM, Helios Nanolab 600i, FEI Co., USA) is used to observe the surface and cross-sectional morphologies of the samples. In addition, the element concentration on the coatings surface are detected by an energy dispersive X-ray spectroscopy (EDS, EDAX, USA) equipped on the SEM system.

Table 1
The labels of MAO coatings formed at different voltages.

Applied voltage (V)	Pulse frequency (Hz)	Duty cycle (%)	Oxidized time (min)	Labels
300	600	8	7	MAO-300
350				MAO-350
400				MAO-400
450				MAO-450
500				MAO-500

2.3.3. Inductively coupled plasma optical emission spectroscopy (ICP-OES)

Inductively coupled plasma optical emission spectroscopy (ICP-OES, Optima 5300DV, Perkin-Elmer, USA) was used to measure the Zn^{2+} release amounts of MAO coatings after immersion in phosphate buffered solution (PBS) solution (pH 7.4) for different time. In the ICP-OES measurement, the Zn ion concentrations of 10 mL PBS solution after immersion of every sample with $10 \times 10\ mm^2$ were measured, and two independent analyses were carried out for each solution.

2.4. Bonding strength test

The bonding strength between coating and titanium substrate was investigated by the direct pull-off method. In the pull-off tests, the samples ($\Phi 30 \times 1\ mm^3$) were bonded to the untreated steel using epoxy resin. The pull-off test was carrying out on an electronic tensile testing machine (Instron 1195, Instron Co., USA). A load to the coating was continually applied on the steel cylinder at a rate of 0.5 mm min^{-1} until the sample was broken. The maximum instant load was recorded. The bonding strength was determined by Eqn (1).

$$P = F_{max}/S \quad (1)$$

Where *Fmax* was the maximum load, *S* is the area of the coating, and *P* is the bonding strength.

2.5. Zn^{2+} release test

The MAO coatings formed at different applied voltages were immersed into 10 mL PBS solution for 1, 3, 5, 7, 11, 13 and 15 days. In the following, the Zn^{2+} release amounts in the PBS solution were measured by ICP-OES. And each group was measured for three times.

2.6. In vitro antibacterial test

The antibacterial ability of the samples is accessed using *E.coli* (ATCC 25922) and *S.aureus* (ATCC 25923). The *E.coli* are placed in the Luria-Bertani (LB) agar plates, and the *S.aureus* was cultured in tryptic soy agar (TSA) plates, and then cultured in the incubator at 37 °C for 24 h. Then the *E.coli* is transferred to the fresh LB plates every 24 h. After cultured in the LB plates for twice times, some active bacterium are transferred into the liquid bacterial medium and cultured in the incubator for 24 h. Then the active bacterial concentrations of *E.coli* are determined by measuring the absorbance at 620 nm (EZ Read 800 Plus Microplate reader, Biochrom). And the bacterial concentrations are adjusted to the final 1.0×10^7 cfu/ml by adding the phosphate buffer saline (PBS) solutions.

Before the bacteria are seeded on all the samples, the samples are placed inside the 24-cell cultural plate and all samples are sterilized by the autoclave at 121 °C for 30min. Then the 30 μL of *E.coli* and *S.aureus* with a concentration of 1.0×10^7 cfu ml^{-1} are seeded on the samples. Then the samples are placed inside the 24-cell culture plate and cultured in the incubator at 37 °C for 24 h. In the following, the samples are washed by the sterilized PBS solution for twice times, and the 100 μL PBS solution are withdrawn from the 10 mL washed PBS solution with the pipette. Finally, the 100 μL solution containing bacteria are transferred to the LB and TSA plates and placed in the incubator at 37 °C for 24 h. The bacterium numbers are measured at optical microscopy, the bacteria number of blank groups are set as A, and the bacteria number of sample groups are set as B. the bacterial rate(R) is calibrated by Eqn. (2) to evaluate the bacterial ability of the samples.

$$R = (A\text{-}B)/A \times 100\% \quad (2)$$

The morphology of *E.coli* and *S.aureus* seeded on the MAO coating was observed by the SEM. In the SEM experiment, the *E.coli* and *S.aureus* were seeded on the MAO coating formed at different applied voltage, cultured in the incubation at 37 °C for 24 h, then fixed with 3%

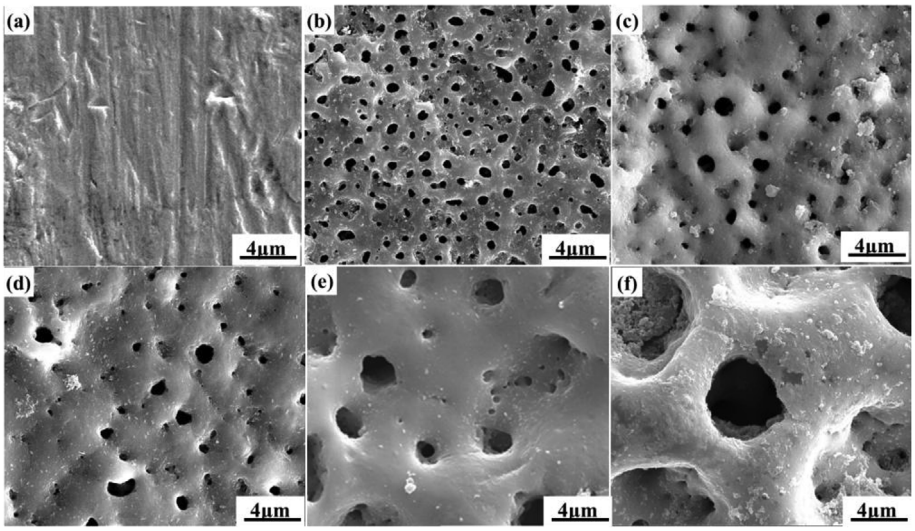

Fig. 1. The SEM images of pure Ti plate and MAO coatings formed at different applied voltages: (a)Ti plate; (b)MAO-300; (c) MAO-350; (d) MAO-400; (e) MAO-450; (f) MAO-500.

glutaraldehyde, dehydrated in a series of ethanol solutions (30, 50, 75, 90, 95 and 100 v/v%) for 10 min each, freeze dried, sputter-coated with gold for SEM observation.

3. Results

3.1. The surface structure and phase compositions of the MAO coatings

Fig. 1 shows the SEM images of pure Ti and MAO coating formed at 300, 350, 400, 450 and 500 V. It was confirmed that the rough and porous surface structure was observed on the Ti plate after MAO treatment. In Fig. 1(b), large numbers of the micropores with the size of about 1 ~ 3 μm were observed on the MAO coating formed at 300 V. However, with the increase of applied voltages (350 ~ 500 V), the average size of the micropores increased, while the density of the micropores decreased on the MAO coating surface as shown in Fig. 1(c)-(f). In addition, the uniformity extent of the micropore size decreased at the applied voltage of 350 ~ 500 V. The results indicated that the applied voltages had an important effect on the surface morphology of the MAO coating.

Fig. 2 gives the XRD patterns of pure Ti plate and MAO coating at different applied voltages (300–500 V). In Fig. 2(a), only Ti peaks at 35.093°, 38.421° and 40.17° were observed on pure Ti plate. After the MAO treatment at different applied voltages (300–500 V), the anatase peaks and rutile peaks were both observed on the MAO coatings as shown in Fig. 2(b)-(f).

Fig. 3 illustrates the cross-section morphology of pure Ti plate and MAO coatings at 300, 350, 400, 450 and 500 V. No apparent discontinuity between MAO coating and Ti substrate was observed at different applied voltages (300–500 V), indicating that the MAO coating had good interfacial bonding strength with the Ti substrate. The thickness of the MAO coating at different applied voltages were shown in Fig. 3(g), with the increase of the applied voltages(300–500 V), the thickness of the MAO coatings increased from 2.3 to 7.5 μm, indicating that the thickness of MAO coatings could be modified by varying the applied voltage. Meanwhile, in Fig. 3 (h), the distributions of Ti and O elements between the titanium substrate and MAO coating had an obvious decrease, which could be used to confirm the thickness of MAO coatings formed at different applied voltages.

Fig.S1 shows that the atomic concentrations of Ca, P and Zn elements in the MAO and MAO-Zn coatings. The atomic concentrations of Ca and P elements in the MAO coating without Zn element were higher than that in the MAO coating without Zn element, indicating that the

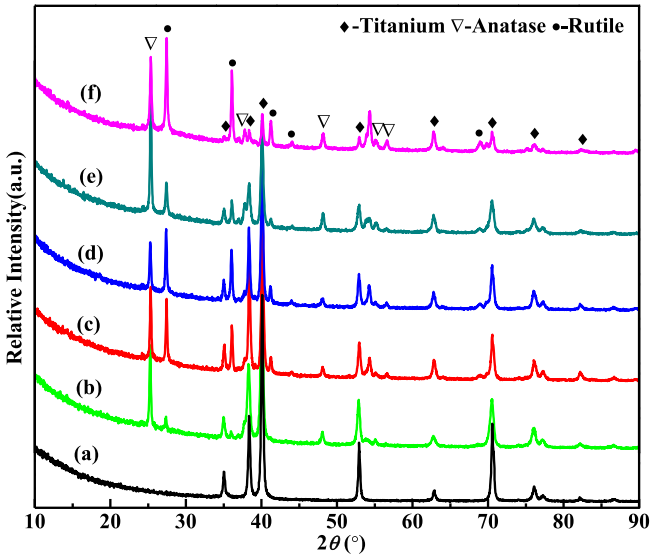

Fig. 2. The XRD patterns of pure Ti plate and MAO coatings formed at different applied voltages: (a)Ti plate; (b)MAO-300; (c)MAO-350; (d)MAO-400; (e)MAO-450; (f)MAO-500.

incorporation of Zn element could affect the concentrations of Ca and P elements. In order to study the effect of the applied voltages on the atomic concentrations of Ca, P and Zn elements. Fig. 4 shows the atomic concentrations of Ca, P and Zn elements on the MAO coatings at 300, 350, 400, 450 and 500 V. In overall, with the increase of the applied voltages, the concentration of Zn element increased, while those of Ca and P elements decreased. However, the concentration of Zn element slightly increased when the voltages varied from 300 to 400 V, while slightly decreased at 450 V. And the decrease of Ca and P elements was not that significantly. With the prolonging of the applied voltages to 500 V, the concentration of Zn element sharply increased, while that of P element sharply decreased. When the applied voltage was ranging from 400 to 500 V, the concentration of Ca element slightly increased. The results revealed that the concentrations of Ca, P and Zn elements in the MAO coatings could be adjusted by varying the applied voltages.

Fig. 5 shows the bonding strength of MAO coatings formed at different applied voltages. According to the calculated results, the applied voltages had a little effect on the bonding strengths between the MAO coatings and the pure Titanium plate, and the bonding strengths were

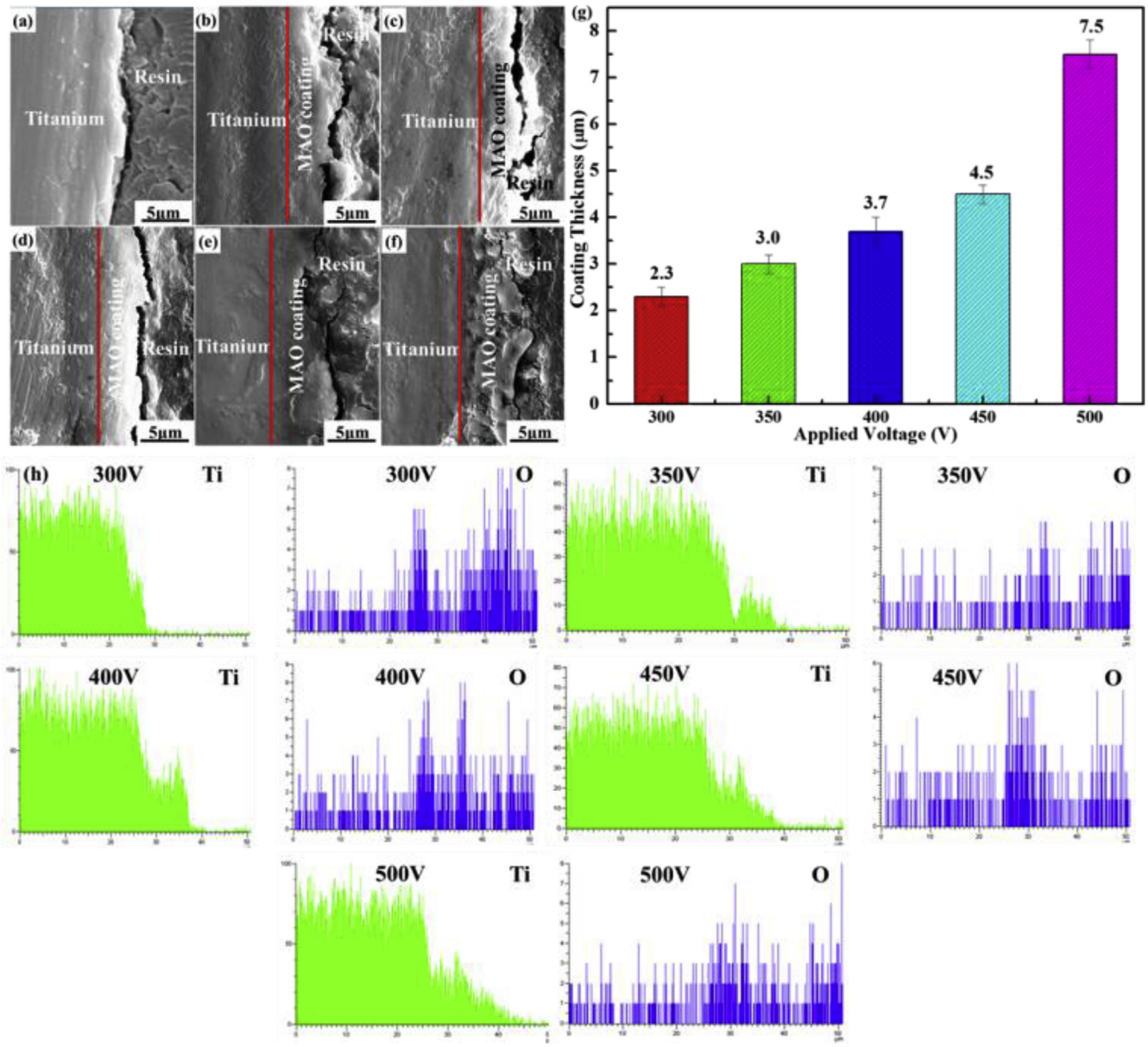

Fig. 3. The cross-section morphology of pure Ti plate and MAO coatings formed at different applied voltages: (a) Ti plate; (b) MAO-300; (c) MAO-350; (d) MAO-400; (e) MAO-450; (f) MAO-500; (g) the thickness of the MAO coatings formed at the different applied voltages; (h) the element distribution of Ti and O elements on the cross-sectional MAO coating formed at different applied voltages.

distributed in the ranging of 45 ~ 50 MPa, which showed the higher interfacial bonding strength, indicating that MAO treatment was an effective method to fabricate the bioactive coating with high bonding strength on the titanium surface.

3.2. The apatite-inducing ability and antibacterial ability of the MAO coatings

Fig. 6 shows the SEM images of pure Ti and MAO coatings formed at 300, 350, 400,450 and 500 V after SBF immersion for 14 and 21days. After SBF immersion for 14 days, no obvious change was observed on the pure Ti plate. Similarly, the rough and porous surfaces remained also clearly observed on the MAO-300, MAO-450 and MAO-500 coatings. However, the new apatite layers were observed on the MAO-350 and MAO-400 coatings. Moreover, the depositions exhibited nano flake-like structure as shown in magnified images of Fig. 6(c) and (d). With the increase of immersion time to 21days, the apatite layers were found on the MAO-300, MAO-350 and MAO-400 coatings. However, the MAO coatings formed at the applied voltage of 450 and 500 V remained in the rough and porous surface, and no obvious apatite layers found.

Fig. 7 gives the XRD patterns of pure Ti plate and MAO coatings formed at the applied voltage of 300, 350, 400,450 and 500 V after SBF immersion for 21days. Generally, the new diffraction peaks of apatite at 25.9° and 32.3° were detected on the MAO-300, MAO-350 and MAO-400 coatings after SBF immersion for 21days. Moreover, the relative intensity ratio of apatite (002) and Ti (101) crystal planes continuously increased from 0.471 to 0.822 on the MAO-300, MAO-350 and MAO-400 coatings. Associated with the SEM and XRD results, the depositions formed on the MAO coatings at 300, 350 and 400 V were apatite. However, the phase compositions of MAO-450 and MAO-500 coating were Ti, anatase and rutile after SBF immersion for 21days, no apatite peaks were found on theses coating surfaces.

Fig. 8 shows the Zn^{2+} released amount of MAO coatings formed at different voltages after PBS immersion for different times. From the Zn^{2+} release curve, it was obviously observed that the Zn^{2+} release amounts from MAO-350, MAO-400 and MAO-450 coatings were slowly

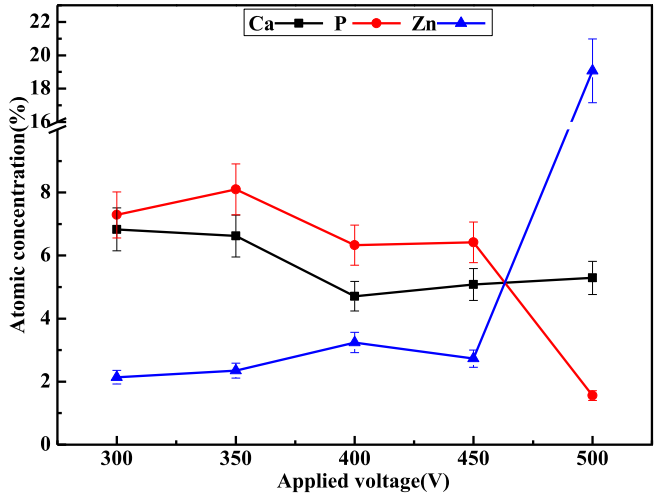

Fig. 4. The atomic concentrations of Ca, P and Zn elements in the MAO coatings formed at different applied voltages.

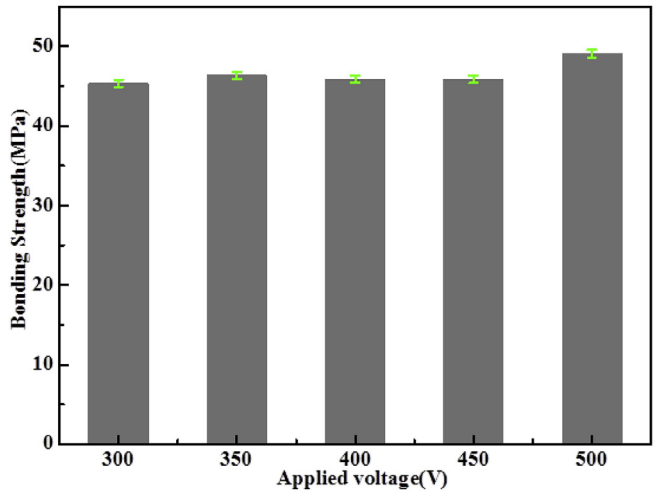

Fig. 5. The bonding strength of the MAO coatings formed at different applied voltages.

increased with the increase of PBS immersion times, while those from the MAO-300 and MAO-500 coatings were obviously increased. Moreover, after PBS immersion for 7days, the Zn^{2+} release rates on the MAO-300 and MAO-500 coatings were higher than those on the MAO-350, MAO-400 and MAO-450 coating surfaces. However, after PBS immersion within 7days, the Zn^{2+} release rates on the MAO coatings had no obviously difference.

Fig. 9 shows the morphology of *E.coli* and *S.aureus* with the concentration of 1.0×10^7 cfu/ml seeded on the pure Ti plate before and after MAO treatment formed at the different applied voltages after culture for 24 h. In Fig. 9 (a), the *E.coli* was rod-shaped and undamaged binary fission when cultured on the pure Ti plate (marked with red arrow in Fig. 9(a)), while the morphology of *E.coli* on the MAO coatings formed at different applied voltages has been damaged (marked with white arrow In Fig. 9(b)-(f)). Similarly, the *S.aureus* displayed round, smooth and intact surface on the pure Ti surface (marked with red arrow in Fig. 9(g)-(l)). However, the morphology of *S.aureus* on the MAO coating surfaces has been deformed and some bacterial cell defers and lysed bacterial cells were noticed on the MAO coating surfaces (marked with white arrow in Fig. 9 (h)-(l)).

Fig.S2 shows the antibacterial rates of MAO and MAO-Zn coatings for *E.coli* and *S.aureus.* Compared to MAO coating without Zn element (MAO), the antibacterial rate of MAO coating for *E.coli* with Zn element (MAO-Zn) had slightly decreased, while that of MAO-Zn coating for *S.aureus* had slightly increased, which had no obvious difference. Fig. 10 shows the optical images and antibacterial rates of the pure Ti plate and MAO coatings formed at different applied voltages for *E.coli* and *S.aureus*. In Fig. 10 (a), compared to the pure Ti, it was clearly observed that the alive bacterial numbers on the MAO coatings formed at the different applied voltages for *E.coli* had significantly decreased, while that for *S.aureus* had slightly decreased. In addition, the survival bacterial number on the MAO-350 coating surface was smallest among the MAO coating surfaces. Likewise, compared to pure Ti, it was clearly seen that the antibacterial rates on the MAO coating surfaces formed at different applied voltages for *E.coli* had obviously increased, while that for *S.aureus* had slightly increased. Moreover, the antibacterial rate on the MAO-350 coating surface was highest among the MAO coatings.

4. Discussions

The MAO coatings containing the different concentrations of Zn elements were successfully fabricated on the titanium surface via varying the applied voltages. Based on the results of SEM and XRD, it was confirmed that the changing of applied voltages was an effective method to optimize the surface and cross-section structure on the MAO coatings surface. With the increase of the applied voltage, the average micropore size on the MAO coating increased, while the micropore intensity on the MAO coating decreased (Fig. 1) [26,27]. Meanwhile, the thickness of the MAO coatings continuously increased (Fig. 3). According to Eqn. (3) as shown in the previous study [28].

$$E_p = \int_0^{t_p} U_p I_p d_t \tag{3}$$

Where E_p was average pulse energy, U_p was applied voltage, I_p was the current and t_p was oxidized time. In this work, with the increase of applied voltages, the average pulse energy E_p can be increased. Meanwhile, there was some weak site in the thin and dense layer. Thus, during MAO treatment process, the as-formed layer was broken down at the weak site, leading to the formation of new layer and micro arc discharge channels. Likewise, the melted depositions were cooled down around the micro arc discharge channels, which resulted in the increase of coating thickness. In addition, the number of weak sites in the coatings reduced with the coating thickness ascending [29], and the reduced number of discharge sites made the dielectric breakdown hard, which needed the higher applied voltage to offer the supplemental energy [30,31].So the dielectric breakdown was easy to occur at the micro arc discharge channels, which leaded to the increase of micropores diameter. In this work, the relative amounts of anatase and rutile phase were also adjusted by the applied voltage (Fig. 2). On one hand, the previous study reported that the addition of $Zn(CHCOO_3)_2$ was beneficial to the formation of rutile TiO_2 phase during MAO treatment [11]. And the micro arc discharge oxidized ability was enhanced during MAO treatment in the electrolyte containing $Zn(CHCOO_3)_2$, which could promote the formation of rutile TiO_2 phase. Compared to the results of previous study, the bonding strength of MAO coatings formed in the electrolyte including $Zn(CHCOO_3)_2$ had been greatly increased, which can reach to the 45 ± 5 MPa due to the high oxidized ability.

Otherwise, with the applied voltages increasing, the concentrations of Zn element steadily increased, while the contents of Ca and P elements slightly decreased (Fig. 4). In the Zn^{2+} release test, it was clearly observed that the Zn element released amount and the released rate from the MAO-300 and MAO-500 coatings were higher than that from the other MAO coating formed at 350,400 and 450 V. Based on the diffusion equation (Eqn. (4)).

$$D = D_0 e^{-Q/RT} \tag{4}$$

Where D was diffusion coefficient, D_0 was frequency factor, Q was diffusion activation energy, R was gas constant (8.314 J/mol·K) and T

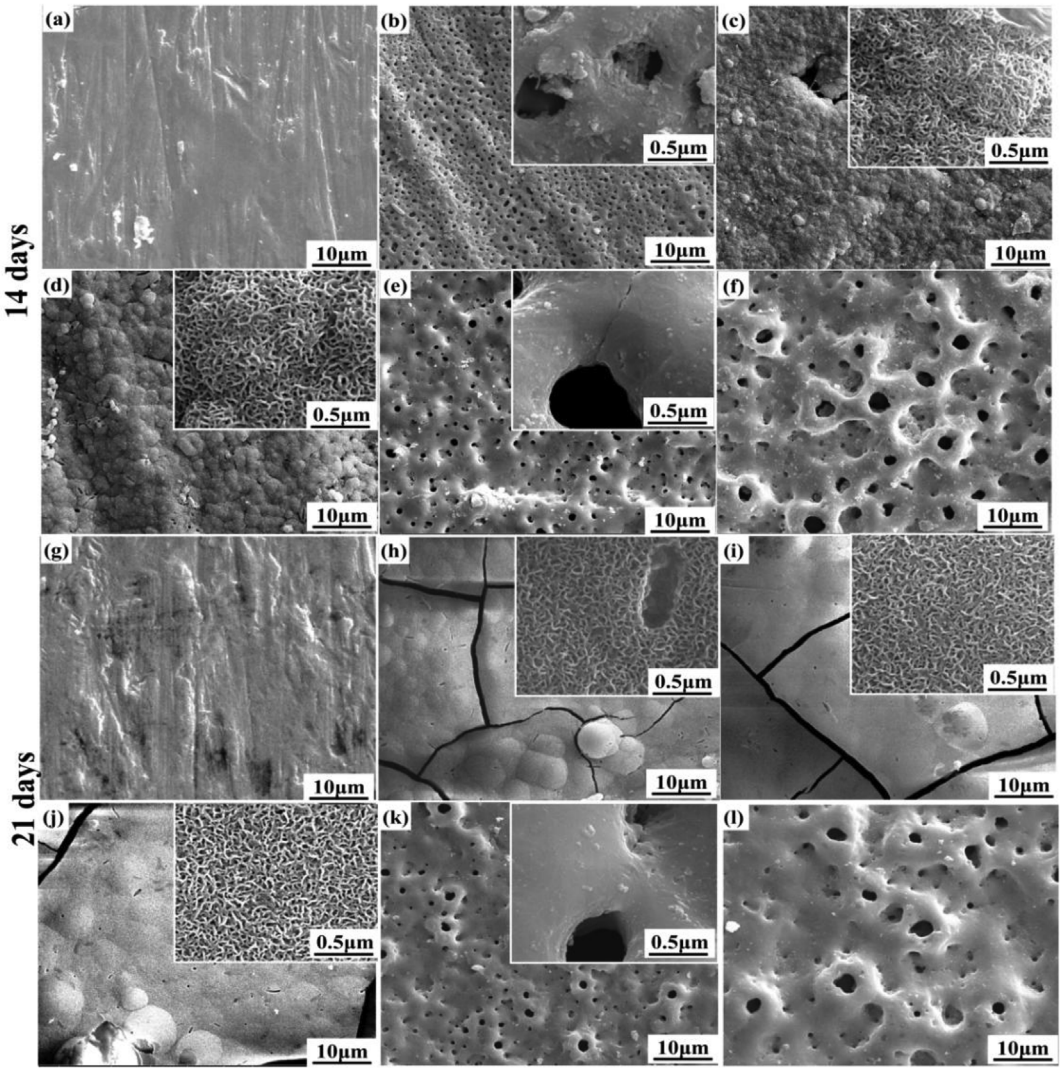

Fig. 6. The SEM images of pure Ti plates and MAO coatings formed at different applied voltages after SBF immersion for 14 and 21 days: (a)–(f) pure Ti plate, MAO-300, MAO-350, MAO-400, MAO-450 and MAO-500 for 14 days; (g)–(l) pure Ti plates, MAO-300, MAO-350, MAO-400, MAO-450 and MAO-500 for 21 days.

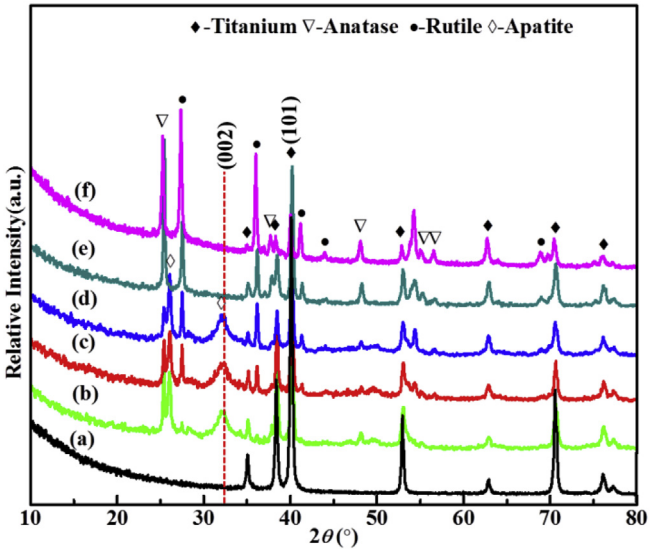

Fig. 7. The XRD patterns of pure Ti plates and MAO coatings formed at different applied voltages after SBF immersion for 21 days. (a) Pure Ti plates, (b) MAO-300, (c) MAO-350, (d) MAO-400, (e) MAO-450, (f) MAO-500.

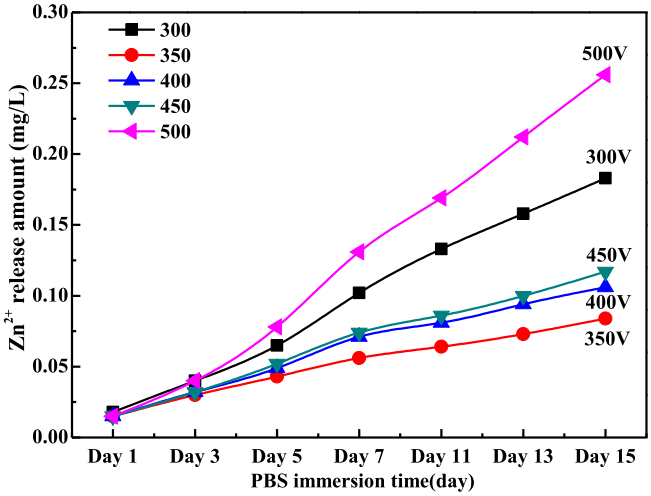

Fig. 8. The Zn^{2+} release amount of MAO coatings formed at different applied voltages after PBS immersion for different times.

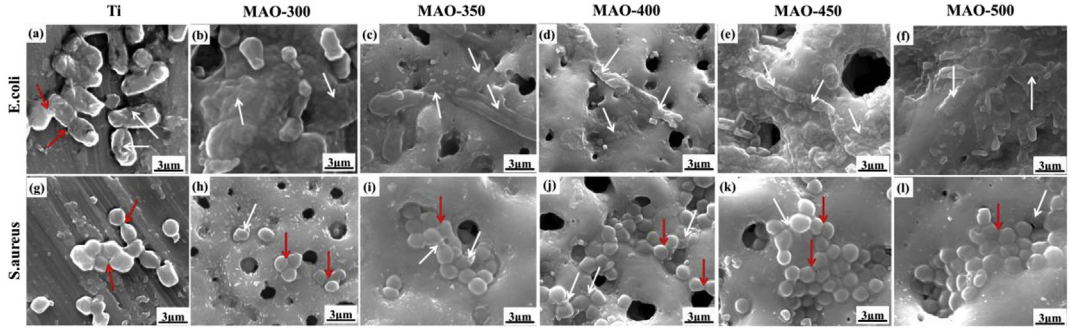

Fig. 9. The morphology of *E.coli* and *S.aureus* with the concentration of 1.0×10^7 cfu/ml seeded on the pure Ti plate before and after MAO treatment formed at different applied voltages: (a)–(f) the SEM images of *E.coli* seeded on pure Ti plate before and after MAO treatment at the applied voltages; (g)–(l) the SEM images of *S.aureus* seeded on the pure Ti plate before and after MAO treatment at applied voltages.

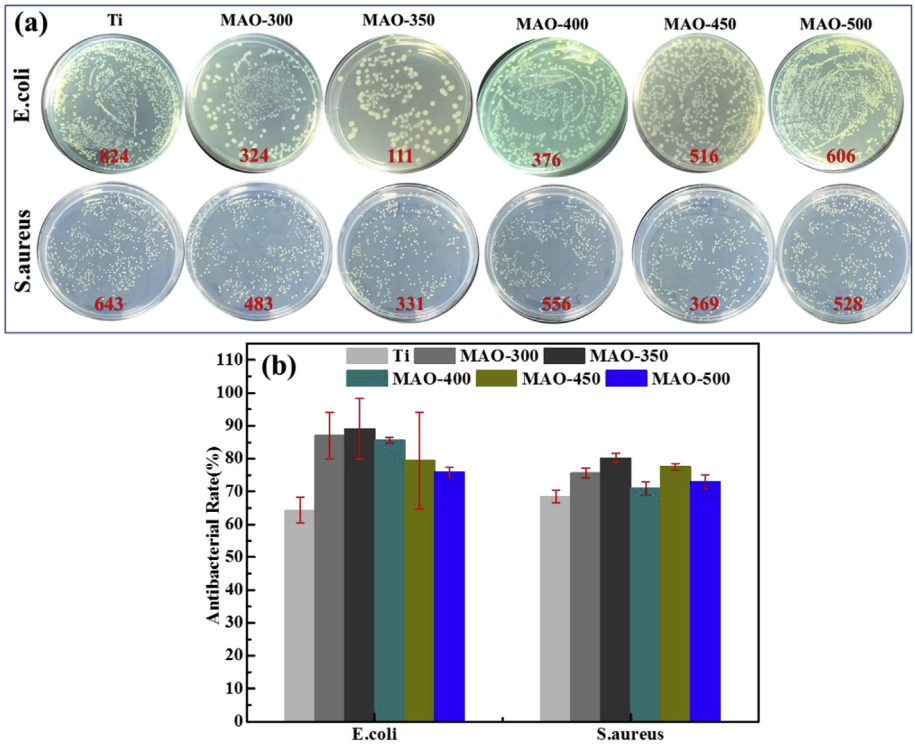

Fig. 10. The optical images (a) and antibacterial rates (b) of pure Ti plate and MAO coatings formed at the different applied voltages for *E.coli and S.aureus*.

was thermodynamic temperature (K). Assuming the formed coatings were dense, the release total amount of Zn element from MAO coating surface was depended on the thickness of MAO coatings as the diffusion coefficient was the same. Due to the existence of micro pores in the MAO coating, in the Zn element release test, the PBS solution in the micro arc discharge channels could increase the diffusion coefficient, and shorten the diffusion distance of Zn element, which was attributed to the higher diffusion coefficient in the PBS solution than that in the MAO coating and higher concentration gradient of Zn element. Thus, in this work, the increased micro pore size and decreased thickness of coating leaded to the Zn element release amount ascending.

In order to evaluate the bioactivity of MAO coating formed at different applied voltage, the apatite-inducing ability was widely used to characterize the bioactivity via in vitro SBF immersion. In this work, the SEM and XRD results confirmed that the MAO-300, MAO-350 and MAO-400 coatings showed good apatite-formation ability after SBF immersion for 21days. The previous study reported that the local supersaturation of Ca and P elements near the coating/SBF interface was increased via the dissolution of Ca and P element from the MAO coatings, which could promote the nucleation and growth of apatite on MAO coating surfaces [32]. In this work, the concentration of the incorporated Ca and P element could be adjusted via the varying applied voltages. During SBF immersion process, the higher content of Ca and P elements were migrated from the MAO-300, MAO-350 and MAO-400 coating surface to the interface, leading to the local supersaturation increasing, which can promote the deposition of apatite on the MAO coating surfaces, indicating the good apatite-inducing ability.

Likewise, the antibacterial ability of MAO coatings formed at the different applied voltages was evaluated by the in vitro antibacterial test. Compared to pure Ti, after MAO treatment, the antibacterial ability on the MAO coating surfaces has been modified. However, with the increase of the applied voltages, the enhancement of the antibacterial ability on the MAO coatings is not in consistent with the increase of Zn elements. As the applied voltage was ranged from the 350–500 V, the antibacterial rates had decreased with the applied voltage ascending, indicating that other incorporated elements such as Ca and P have a positive effect on the improvement of antibacterial ability. In this work, it was concluded that the incorporation of Zn element could affect the concentration of Ca and P elements in the MAO-Zn coating compared to the MAO coating. Besides, the

concentrations of Ca and P elements in the MAO coating were higher than that in the MAO-Zn coating as shown in Fig.S1. If the Zn element was the key parameter to improve the antibacterial ability of MAO coating, the introduction of Zn element could greatly improve the antibacterial ability of MAO coating. However, the antibacterial ability for *E.coli* of MAO coating was better than that of MAO-Zn coating as shown in Fig.S2, while that for *S.aureus* of MAO coating was lower than that of MAO-Zn coating. Thus, the Ca and P element had a positive effect on the antibacterial ability for *E.coli*, and the S.aureus was more sensitive than *E.coli* to Zn element. Meanwhile, Alves S.A [10] compared the antibacterial ability of Ca and P-incorporated TiO_2 nanotubes and Ca, P and Zn-incorporated TiO_2 nanotubes, which revealed the Ca and P elements could affect the bacteria viability. Thus, the enhancement of the antibacterial ability on the MAO coating are not only relied on the comprehensive effect of incorporated elements in the MAO coatings but also the surface porous topological structure. Meanwhile, the previous studies [11,13,14] reported that the contents of Zn, Ca and P elements on the MAO coating surface have a comprehensive effect on the antibacterial ability for *E.coli and S.aureus*. Thus, in this work, the antibacterial ability is promoted via adjusting the contents of Zn, Ca and P elements in the MAO coatings and modifying the surface structure of MAO coating.

5. Conclusions

The Zn-incorporated MAO coatings are successfully fabricated on the titanium surface in the electrolyte containing $Zn(CH_3COO)_2$. The MAO coatings containing the different concentrations of Zn, Ca and P elements are formed at the different applied voltages (300, 350, 400, 450 and 500 V). With the increase of the applied voltages, the average size of the micro-pores significantly increases, while the density of the micro-pores obviously decreases. Meanwhile, the thickness of the MAO coatings continuously increases. In addition, the concentrations of Ca, P and Zn elements are adjusted via the changing of the applied voltages. Compared to pure titanium, after MAO treatment, the apatite-inducing ability of MAO-350 and MAO-400 coating have been improved. Meanwhile, the antibacterial tests reveal that the Ca, P and Zn-incorporated MAO coatings show the good antibacterial ability. Moreover, the MAO coating has higher bonding strength. Thus, the apatite-inducing ability and antibacterial ability on the MAO coating are affected by the comprehensive effect of the incorporated elements and surface property.

Acknowledgments

This work was financially supported by Heilongjiang Provincial Youth Science Foundation (QC2013C043), National Basic Science Research Program (2012CB933900) and the Fundamental Research Funds for the Central Universities (Grant no.HIT.NSRIF.2014002).

Appendix A. Supplementary data

Supplementary data related to this article can be found at http://dx.doi.org/10.1016/j.bioactmat.2018.06.001.

References

[1] D. Wei, W. Feng, Q. Du, R. Zhou, B. Li, Y. Wang, et al., Titania nanotube/nanobrushite composited bioactive coating with micro/nanotopography on titanium formed by anodic oxidation and hydrothermal treatment, Ceram. Int. 41 (2015) 13115–13125.
[2] R. Manoj Kumar, K.K. Kuntal, S. Singh, P. Gupta, B. Bhushan, P. Gopinath, et al., Electrophoretic deposition of hydroxyapatite coating on Mg–3Zn alloy for orthopaedic application, Surf. Coating. Technol. 287 (2016) 82–92.
[3] R.I. Asri, W.S. Harun, M.A. Hassan, S.A. Ghani, Z. Buyong, A review of hydroxyapatite-based coating techniques: sol-gel and electrochemical depositions on biocompatible metals, J Mech Behav Biomed Mater 57 (2015) 95–108.
[4] W. Zimmerli, Clinical presentation and treatment of orthopaedic implant-associated infection, J. Intern. Med. 276 (2) (2014) 111–119.
[5] S. Pouraghaei, F. Moztarzadeh, N. Nezafati, et al., Synthesis and characterization of silver-containing sol-gel derived bioactive glass coating, Protect. Met. Phys. Chem. Surface 52 (2) (2016) 285–290.
[6] S.L. Iconaru, A.M. Prodan, N. Buton, et al., Structural characterization and antifungal studies of zinc-doped hydroxyapatite coatings, Molecules 22 (4) (2017) 604.
[7] Y. Huang, M. Hao, X. Nian, et al., Strontium and copper co-substituted hydroxyapatite-based coatings with improved antibacterial activity and cytocompatibility fabricated by electrodeposition, Ceram. Int. 42 (10) (2016) 11876–11888.
[8] Y. Huang, X. Zhang, H. Zhang, et al., Fabrication of silver-and strontium-doped hydroxyapatite/TiO_2 nanotube bilayer coatings for enhancing bactericidal effect and osteoinductivity, Ceram. Int. 43 (1) (2017) 992–1007.
[9] Y. Huang, Z. Xu, X. Zhang, et al., Nanotube-formed Ti substrates coated with silicate/silver co-doped hydroxyapatite as prospective materials for bone implants, J. Alloy. Comp. 697 (2017) 182–199.
[10] S.A. Alves, A.R. Ribeiro, S. Gemini-Piperni, et al., TiO_2 nanotubes enriched with calcium, phosphorous and zinc: promising bio-selective functional surfaces for osseointegrated titanium implants, RSC Adv. 7 (78) (2017) 49720–49738.
[11] H. Hu, W. Zhang, Y. Qiao, et al., Antibacterial activity and increased bone marrow stem cell functions of Zn-incorporated TiO_2 coatings on titanium, Acta Biomaterialia 8 (2) (2012) 904–915.
[12] L. Zhang, J. Guo, T. Yan, et al., Fibroblast responses and antibacterial activity of Cu and Zn co-doped TiO_2 for percutaneous implants, Appl. Surf. Sci. 434 (2018) 633–642.
[13] L. Ren, X. Lin, L. Tan, et al., Effect of surface coating on antibacterial behavior of magnesium based metals, Mater. Lett. 65 (23) (2011) 3509–3511.
[14] B.H. Zhao, W. Zhang, D.N. Wang, et al., Effect of Zn content on cytoactivity and bacteriostasis of micro-arc oxidation coatings on pure titanium, Surf. Coating. Technol. 228 (2013) S428–S432.
[15] X. Zhang, H. Wang, J. Li, et al., Corrosion behavior of Zn-incorporated antibacterial TiO_2 porous coating on titanium, Ceram. Int. 42 (15) (2016) 17095–17100.
[16] W.H. Chang, B. Qu, A.D. Liao, et al., In vitro biocompatibility and antibacterial behavior of anodic coatings fabricated in an organic phosphate containing solution on Mg-1.0Ca alloys, Surf. Coating. Technol. 289 (2016) 75–84.
[17] W. Zhu, Z. Zhang, B. Gu, et al., Biological activity and antibacterial property of nano-structured TiO_2 coating incorporated with Cu prepared by micro-arc oxidation, J. Mater. Sci. Technol. 29 (3) (2013) 237–244.
[18] Q. Wu, J. Li, W. Zhang, et al., Antibacterial property, angiogenic and osteogenic activity of Cu-incorporated TiO_2 coating, J. Mater. Chem. B 2 (39) (2014) 6738–6748.
[19] X. He, X. Zhang, L. Bai, et al., Antibacterial ability and osteogenic activity of porous Sr/Ag-containing TiO_2 coatings, Biomed. Mater. 11 (4) (2016) 045008.
[20] J.L. Lee, K.N. Kuo, T.L. Sung, et al., Preparation of antibacterial ceramic coatings containing Ag on titanium alloy by use of microarc oxidation, IEEE Trans. Plasma Sci. 44 (12) (2016) 3179–3182.
[21] X. He, X. Zhang, X. Wang, et al., Review of antibacterial activity of titanium-based implants' surfaces fabricated by micro-arc oxidation, Coatings 7 (3) (2017) 45.
[22] A. Bari, N. Bloise, S. Fiorilli, et al., Copper-containing mesoporous bioactive glass nanoparticles as multifunctional agent for bone regeneration, Acta Biomater. 55 (2017) 493–504.
[23] J. Xu, G. Ding, J. Li, et al., Zinc-ion implanted and deposited titanium surfaces reduce adhesion of Streptococccus mutans, Appl. Surf. Sci. 256 (24) (2010) 7540–7544.
[24] B.M. Hidalgo-Robatto, M. López-Álvarez, A.S. Azevedo, et al., Pulsed laser deposition of copper and zinc doped hydroxyapatite coatings for biomedical applications, Surf. Coating. Technol. 333 (2018) 168–177.
[25] A. Oyane, H.M. Kim, T. Furuya, et al., Preparation and assessment of revised simulated body fluids, J. Biomed. Mater. Res. 65 (2) (2003) 188–195.
[26] E. Matykina, A. Berkani, P. Skeldon, et al., Real-time imaging of coating growth during plasma electrolytic oxidation of titanium, Electrochim. Acta 53 (4) (2007) 1987–1994.
[27] D. Veys-Renaux, E. Rocca, Initial stages of multi-phased aluminium alloys anodizing by MAO: micro-arc conditions and electrochemical behaviour, J. Solid State Electrochem. 19 (10) (2015) 3121–3129.
[28] Y.M. Wang, D.C. Jia, L.X. Guo, et al., Effect of discharge pulsating on microarc oxidation coatings formed on Ti6Al4V alloy, Mater. Chem. Phys. 90 (1) (2005) 128–133.
[29] S. Moon, Y. Jeong, Generation mechanism of micro discharges during plasma electrolytic oxidation of Al in aqueous solutions, Corrosion Sci. 51 (7) (2009) 1506–1512.
[30] A. Nominé, S.C. Troughton, A.V. Nominé, et al., High speed video evidence for localized discharge cascades during plasma electrolytic oxidation, Surf. Coating. Technol. 269 (2015) 125–130.
[31] L. Wang, L. Chen, Z. Yan, et al., Optical emission spectroscopy studies of discharge mechanism and plasma characteristics during plasma electrolytic oxidation of magnesium in different electrolytes, Surf. Coating. Technol. 205 (6) (2010) 1651–1658.
[32] M. Fengcang, L. Pimg, L. Wei, et al., Effect of applied voltage on the microstructure and bioactivity of MAO film on Ti substrate, Mater. Trans. 54 (9) (2013) 1800–1804.